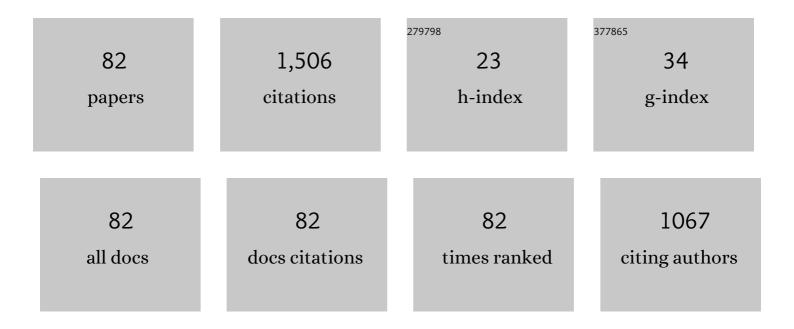
List of Publications by Year in descending order

Source: https://exaly.com/author-pdf/4698183/publications.pdf Version: 2024-02-01



Ισι Ηοιιςκα

#	Article	IF	CITATIONS
1	Reactive magnetron sputtering of hard Si–B–C–N films with a high-temperature oxidation resistance. Journal of Vacuum Science and Technology A: Vacuum, Surfaces and Films, 2005, 23, 1513-1522.	2.1	76
2	Process stabilization and a significant enhancement of the deposition rate in reactive high-power impulse magnetron sputtering of ZrO2 and Ta2O5 films. Surface and Coatings Technology, 2013, 236, 550-556.	4.8	72
3	Benefits of the controlled reactive high-power impulse magnetron sputtering of stoichiometric ZrO2 films. Vacuum, 2015, 114, 131-141.	3.5	56
4	Influence of substrate bias voltage on structure and properties of hard Si–B–C–N films prepared by reactive magnetron sputtering. Diamond and Related Materials, 2007, 16, 29-36.	3.9	55
5	Overview of optical properties of Al2O3 films prepared by various techniques. Thin Solid Films, 2012, 520, 5405-5408.	1.8	53
6	High-rate reactive high-power impulse magnetron sputtering of hard and optically transparent HfO 2 films. Surface and Coatings Technology, 2016, 290, 58-64.	4.8	49
7	Significant improvement of the performance of ZrO2/V1-W O2/ZrO2 thermochromic coatings by utilizing a second-order interference. Solar Energy Materials and Solar Cells, 2019, 191, 365-371.	6.2	46
8	Effect of the gas mixture composition on high-temperature behavior of magnetron sputtered Si–B–C–N coatings. Surface and Coatings Technology, 2008, 203, 466-469.	4.8	42
9	Controlled reactive HiPIMS—effective technique for low-temperature (300 °C) synthesis of VO ₂ films with semiconductor-to-metal transition. Journal Physics D: Applied Physics, 2017, 50, 38LT01.	2.8	38
10	Properties of nanocrystalline Al–Cu–O films reactively sputtered by DC pulse dual magnetron. Applied Surface Science, 2011, 258, 1762-1767.	6.1	36
11	Effect of nitrogen content on electronic structure and properties of SiBCN materials. Acta Materialia, 2011, 59, 2341-2349.	7.9	36
12	Atomistic simulations of the characteristics of TiSiN nanocomposites of various compositions. Surface and Coatings Technology, 2009, 203, 3348-3355.	4.8	35
13	Effect of B and the Si/C ratio on high-temperature stability of Si–B–C–N materials. Europhysics Letters, 2006, 76, 512-518.	2.0	34
14	Characterization of thermochromic VO2 (prepared at 250 ŰC) in a wide temperature range by spectroscopic ellipsometry. Applied Surface Science, 2017, 421, 529-534.	6.1	34
15	Pathway for a low-temperature deposition of α-Al2O3: A molecular dynamics study. Surface and Coatings Technology, 2013, 235, 333-341.	4.8	30
16	Experimental and molecular dynamics study of the growth of crystalline TiO2. Journal of Applied Physics, 2012, 112, 073527.	2.5	29
17	High-rate reactive high-power impulse magnetron sputtering of Ta–O–N films with tunable composition and properties. Thin Solid Films, 2014, 566, 70-77.	1.8	29
18	High-performance thermochromic VO2-based coatings with a low transition temperature deposited on glass by a scalable technique. Scientific Reports, 2020, 10, 11107.	3.3	29

#	Article	IF	CITATIONS
19	Properties of thermochromic VO2 films prepared by HiPIMS onto unbiased amorphous glass substrates at a low temperature of 300â€Â°C. Thin Solid Films, 2018, 660, 463-470.	1.8	26
20	Ab initiosimulations of nitrogen evolution in quenchedCNxand SiBCN amorphous materials. Physical Review B, 2005, 72, .	3.2	25
21	Trends in formation energies and elastic moduli of ternary and quaternary transition metal nitrides. Journal of Materials Science, 2013, 48, 7642-7651.	3.7	25
22	A study of the microstructure evolution of hard Zr–B–C–N films by high-resolution transmission electron microscopy. Acta Materialia, 2014, 77, 212-222.	7.9	25
23	Microstructure of hard and optically transparent HfO2 films prepared by high-power impulse magnetron sputtering with a pulsed oxygen flow control. Thin Solid Films, 2016, 619, 239-249.	1.8	25
24	Improved performance of thermochromic VO2/SiO2 coatings prepared by low-temperature pulsed reactive magnetron sputtering: Prediction and experimental verification. Journal of Alloys and Compounds, 2018, 767, 46-51.	5.5	24
25	Mechanical and optical properties of quaternary Si–B–C–N films prepared by reactive magnetron sputtering. Thin Solid Films, 2008, 516, 7286-7293.	1.8	23
26	Atom-by-atom simulations of chemical vapor deposition of nanoporous hydrogenated silicon nitride. Journal of Applied Physics, 2010, 107, .	2.5	22
27	Pulsed reactive magnetron sputtering of high-temperature Si–B–C–N films with high optical transparency. Surface and Coatings Technology, 2013, 226, 34-39.	4.8	22
28	Structure and properties of Hf-O-N films prepared by high-rate reactive HiPIMS with smoothly controlled composition. Ceramics International, 2017, 43, 5661-5667.	4.8	22
29	Bonding statistics and electronic structure of novel Si–B–C–N materials: <i>Ab initio</i> calculations and experimental verification. Journal of Vacuum Science and Technology A: Vacuum, Surfaces and Films, 2007, 25, 1411-1416.	2.1	21
30	Hard multifunctional Hf–B–Si–C films prepared by pulsed magnetron sputtering. Surface and Coatings Technology, 2014, 257, 301-307.	4.8	20
31	Effect of the Si content on the microstructure of hard, multifunctional Hf–B–Si–C films prepared by pulsed magnetron sputtering. Applied Surface Science, 2015, 357, 1343-1354.	6.1	20
32	Thermal, mechanical and electrical properties of hard B4C, BCN, ZrBC and ZrBCN ceramics. Ceramics International, 2016, 42, 4361-4369.	4.8	20
33	Tribological properties and oxidation resistance of tungsten and tungsten nitride films at temperatures up to 500â€ ⁻ °C. Tribology International, 2019, 132, 211-220.	5.9	20
34	The effect of argon on the structure of amorphous SiBCN materials: an experimental andab initiostudy. Journal of Physics Condensed Matter, 2006, 18, 2337-2348.	1.8	19
35	Design and reactive magnetron sputtering of thermochromic coatings. Journal of Applied Physics, 2022, 131, .	2.5	19
36	Effect of implanted argon on hardness of novel magnetron sputtered Si–B–C–N materials: experiments andab initiosimulations, Journal of Physics Condensed Matter, 2007, 19, 196228	1.8	17

#	Article	IF	CITATIONS
37	Formation and behavior of unbonded hydrogen in a-C:H of various compositions and densities. Surface and Coatings Technology, 2009, 203, 3770-3776.	4.8	15
38	Molecular dynamics study of the growth of crystalline ZrO2. Surface and Coatings Technology, 2016, 304, 23-30.	4.8	15
39	Effect of N and Zr content on structure, electronic structure and properties of ZrBCN materials: An ab-initio study. Thin Solid Films, 2013, 542, 225-231.	1.8	14
40	Dependence of characteristics of MSiBCN (M = Ti, Zr, Hf) on the choice of metal element: Experimental and ab-initio study. Thin Solid Films, 2016, 616, 359-365.	1.8	14
41	Magnetron sputtered Hf–B–Si–C–N films with controlled electrical conductivity and optical transparency, and with ultrahigh oxidation resistance. Thin Solid Films, 2018, 653, 333-340.	1.8	14
42	Quantitative investigation of the role of high-energy particles in Al2O3 thin film growth: A molecular-dynamics study. Surface and Coatings Technology, 2014, 254, 131-137.	4.8	13
43	Force field for realistic molecular dynamics simulations of ZrO 2 growth. Computational Materials Science, 2016, 111, 209-217.	3.0	13
44	Enhancement of the deposition rate in reactive mid-frequency ac magnetron sputtering of hard and optically transparent ZrO 2 films. Surface and Coatings Technology, 2018, 336, 54-60.	4.8	12
45	High-rate reactive high-power impulse magnetron sputtering of transparent conductive Al-doped ZnO thin films prepared at ambient temperature. Thin Solid Films, 2019, 679, 35-41.	1.8	12
46	Molecular dynamics and experimental study of the growth, structure and properties of Zr–Cu films. Journal of Alloys and Compounds, 2020, 828, 154433.	5.5	12
47	Pulsed Magnetron Sputtering of Strongly Thermochromic VO2-Based Coatings with a Transition Temperature of 22 ŰC onto Ultrathin Flexible Glass. Coatings, 2020, 10, 1258.	2.6	11
48	Dependence of structure and properties of hard nanocrystalline conductive films MBCN (M = Ti, Zr,) Tj ETQq0 0	0 rgBT /0\	verlock 10 Tf
49	Effect of annealing on structure and properties of Ta–O–N films prepared by high power impulse magnetron sputtering. Ceramics International, 2019, 45, 9454-9461.	4.8	10
50	lon-flux characteristics during low-temperature (300 °C) deposition of thermochromic VO ₂ films using controlled reactive HiPIMS. Journal Physics D: Applied Physics, 2019, 52, 025205.	2.8	10
51	Transfer of the sputter technique for deposition of strongly thermochromic VO2-based coatings on ultrathin flexible glass to large-scale roll-to-roll device. Surface and Coatings Technology, 2022, 442, 128273.	4.8	10
52	SiBCN materials for high-temperature applications: Atomistic origin of electrical conductivity. Journal of Applied Physics, 2010, 108, .	2.5	9
53	Dependence of the ZrO2 growth on the crystal orientation: growth simulations and magnetron sputtering. Applied Surface Science, 2022, 572, 151422.	6.1	9
54	Ab initiomodeling of complex amorphous transition-metal-based ceramics. Journal of Physics Condensed Matter, 2011, 23, 025502.	1.8	8

⁵⁴

#	Article	IF	CITATIONS
55	In-Ga-Zn-O thin films with tunable optical and electrical properties prepared by high-power impulse magnetron sputtering. Thin Solid Films, 2018, 658, 27-32.	1.8	8
56	Relationships between composition and properties of (Cr/Ti)SiN and (Cr/Ti)CN alloys: anab initiostudy. Journal of Physics Condensed Matter, 2009, 21, 285302.	1.8	7
57	Reactive high-power impulse magnetron sputtering of ZrO2 films with gradient ZrOx interlayers on pretreated steel substrates. Journal of Vacuum Science and Technology A: Vacuum, Surfaces and Films, 2017, 35, 031503.	2.1	7
58	Effect of energetic particles on pulsed magnetron sputtering of hard nanocrystalline MBCN (M = Ti, Zr,) Tj	ETQq0 0 (1.8) rgBT /Overloo
59	Dependence of characteristics of Hf(M)SiBCN (MÂ=ÂY, Ho, Ta, Mo) thin films on the M choice: Ab-initio and experimental study. Acta Materialia, 2021, 206, 116628.	7.9	7
60	Microstructure of high-performance thermochromic ZrO2/V0.984W0.016O2/ZrO2 coating with a low transition temperature (22°C) prepared on flexible glass. Surface and Coatings Technology, 2021, 424, 127654.	4.8	7
61	lon-bombardment characteristics during deposition of TiN films using a grid-assisted magnetron system with enhanced plasma potential. Vacuum, 2007, 81, 1109-1113.	3.5	6
62	Relationships between the distribution of O atoms on partially oxidized metal (Al, Ag, Cu, Ti, Zr, Hf) surfaces and the adsorption energy: A density-functional theory study. Journal of Applied Physics, 2017, 121, 225303.	2.5	6
63	Ageing resistance of SiBCN ceramics. Ceramics International, 2015, 41, 7921-7928.	4.8	5
64	Thermal stability of structure, microstructure and enhanced properties of Zr–Ta–O films with a low and high Ta content. Surface and Coatings Technology, 2018, 335, 95-103.	4.8	5
65	Maximum N content in a-CNx by ab-initio simulations. Acta Materialia, 2019, 174, 189-194.	7.9	5
66	Self-organization of vapor-deposited polyolefins at the solid/vacuum interface. Progress in Organic Coatings, 2020, 143, 105630.	3.9	5
67	Tunable composition and properties of Al-O-N films prepared by reactive deep oscillation magnetron sputtering. Surface and Coatings Technology, 2020, 392, 125716.	4.8	5
68	Extraordinary high-temperature behavior of electrically conductive Hf7B23Si22C6N40 ceramic film. Surface and Coatings Technology, 2020, 391, 125686.	4.8	5
69	Distribution of O atoms on partially oxidized metal targets, and the consequences for reactive sputtering of individual metal oxides. Surface and Coatings Technology, 2020, 392, 125685.	4.8	5
70	A study on the energy distribution for grid-assisting magnetron sputtering. Surface and Coatings Technology, 2005, 200, 421-424.	4.8	4
71	Toward colorless smart windows. Solar Energy Materials and Solar Cells, 2021, 230, 111210.	6.2	4
72	Hard and electrically conductive multicomponent diboride-based films with high thermal stability. Ceramics International, 2021, , .	4.8	4

5

#	Article	IF	CITATIONS
73	Thermal stability and transformation phenomena in magnetron sputtered Al–Cu–O films. Ceramics International, 2015, 41, 6020-6029.	4.8	3
74	Force field for realistic molecular dynamics simulations of TiO 2 growth. Computational Materials Science, 2017, 134, 1-7.	3.0	3
75	Enhancement of high-temperature oxidation resistance and thermal stability of hard and optically transparent Hf–B–Si–C–N films by Y or Ho addition. Journal of Non-Crystalline Solids, 2021, 553, 120470.	3.1	3
76	Vacancies and substitutional defects in multicomponent diboride Ti _{0.25} Zr _{0.25} Hf _{0.25} Ta _{0.25} B ₂ : first-principle study. Journal of Physics Condensed Matter, 2022, 34, 095901.	1.8	3
77	Stress reduction in cubic boron nitride by oxygen addition: Explanation of the mechanism by ab-initio simulations. Surface and Coatings Technology, 2012, 206, 2541-2544.	4.8	2
78	Maximum Achievable N Content in Atom-by-Atom Growth of Amorphous Si–C–N. ACS Applied Materials & Interfaces, 2020, 12, 41666-41673.	8.0	2
79	Maximum Achievable N Content in Atom-by-Atom Growth of Amorphous Si-B-C-N Materials. Materials, 2021, 14, 5744.	2.9	2
80	Bixbyite-Ta2N2O film prepared by HiPIMS and postdeposition annealing: Structure and properties. Journal of Vacuum Science and Technology A: Vacuum, Surfaces and Films, 2020, 38, .	2.1	1
81	Strong effect of the interaction potential cut-off on the crystallinity of films grown by simulations. Molecular Simulation, 2017, 43, 1436-1441.	2.0	0
82	Multifunctional MoOx and MoOxNy films with 2.5 < x < 3.0 and y < 0.2 prepared using controlled reactive deep oscillation magnetron sputtering. Thin Solid Films, 2021, 717, 138442.	1.8	0